

Study on mechanical and micro structural properties of spin arc welding in Hastelloy C-2000

Ilavarasan Karthic Subramaniyan^{a,*}, Poosari Kumaravel Srividhya^a, Jothi Kesavan^a

^aDepartment of Mechanical Engineering, Periyar Maniammai Institute of Science & Technology (Deemed to be University), Thanjavur 613 403, India

(*Corresponding author: karthiksubu2610@gmail.com)

Submitted: 22 April 2023; Accepted: 1 December 2023; Available On-line: 3 January 2024

ABSTRACT: Nickel-based Hastelloy C-2000 is widely used in the aerospace, chemical, and medicinal sectors. Investigating the potential efficacy of the spin arc welding process on Hastelloy C-2000 was the main focus of this study. In spin arc welding the centrifugal force has been obtained in the fusion zone, thus the weldbead quality increases. Weld current, rotating speed, and spin diameter are all separate parameters used in the welding procedure. The microstructural investigation was carried out using optical microscopy, X-Ray Diffraction (XRD), and field emission scanning electron microscopy (FESEM). The mechanical characteristics of the welded specimens were examined closely. Spin Arc Welding ultimate tensile strength (UTS), hardness value (HV), and impact experiments were compared to those of the Multi-pass Pulsed Current Gas Tungsten Arc welding method (MPCGTAW). In 27 tests, increasing the current and rotating speed resulted in greater penetration depth and weld height. The width of the weld was found to be a little high, with a spinning diameter of 2 mm. In comparison, samples 5 and 15 were found to have better hardness, tensile strength, and toughness, especially with suitable welding parameters such as current (120 I and 140 I), speed (1800 rpm), and spin diameter (2 mm and 3 mm). A microstructural study showed no grain segregation, contributing to the material's increased hardness and tensile strength. The novel findings of the present study suggest that spin arc welding might be superior for various Hastelloy C-2000 connections that might have great applications in industries.

KEYWORDS: ERNiCrMo-4; Hastelloy C-2000; Mechanical strength; MPCGTAW; Spin arc welding

Citation/Citar como: Karthic Subramaniyan, I.; Srividhya, P.K.; Kesavan, J. (2023). "Study on mechanical and micro structural properties of spin arc welding in Hastelloy C-2000". *Rev. Metal.* 59(4): e252. <https://doi.org/10.3989/revmetalm.252>

RESUMEN: *Estudio de las propiedades mecánicas y microestructurales de la soldadura por arco helicoidal en Hastelloy C-2000.* La aleación base níquel Hastelloy C-2000 se utiliza ampliamente en los sectores aeroespacial, químico y medicinal. El objetivo principal de este estudio era investigar la eficacia potencial del proceso de soldadura por arco giratorio en el Hastelloy C-2000. En la soldadura por arco giratorio se ha obtenido una fuerza centrífuga en la zona de fusión, con lo que se aumenta la calidad del cordón de soldadura. La corriente de soldadura, la velocidad de rotación y el diámetro de giro son parámetros independientes utilizados en el procedimiento de soldadura. La investigación microestructural se llevó a cabo utilizando microscopía óptica, difracción

Copyright: © 2023 CSIC. This is an open-access article distributed under the terms of the Creative Commons Attribution 4.0 International (CC BY 4.0) License.

de rayos X (DRX) y microscopía electrónica de barrido (MEB). Se examinaron minuciosamente las características mecánicas de las muestras soldados. Se comparó la resistencia máxima (UTS), el valor de dureza (HV) y los experimentos de impacto de la soldadura por arco giratorio con los del método de soldadura por arco de tungsteno con gas de corriente pulsada multipaso (MPCGTAW). En 27 pruebas, el aumento de la corriente y de la velocidad de rotación dio lugar a una mayor profundidad de penetración y altura de la soldadura. La anchura de la soldadura resultó un poco elevada, con un diámetro de hilatura de 2 mm. En comparación, se observó que las muestras 5 y 15 tenían mejor dureza, resistencia a la tracción y tenacidad, especialmente con parámetros de soldadura adecuados, como la corriente (120 I y 140 I), la velocidad (1800 rpm) y el diámetro de giro (2 mm y 3 mm). Un estudio microestructural mostró la ausencia de segregación en el grano, lo que contribuyó al aumento de la dureza y la resistencia a la tracción del material. Los resultados novedosos del presente estudio sugieren que la soldadura por arco helicoidal podría ser superior para diversas uniones de Hastelloy C-2000 que podrían tener grandes aplicaciones en la industria.

PALABRAS CLAVE: ERNiCrMo-4; Hastelloy C-2000; MPCGTAW; Resistencia mecánica; Soldadura por arco rotativo

ORCID ID: I. Karthic Subramaniyan (<https://orcid.org/0000-0002-9995-4084>); P.K. Srividhya (<https://orcid.org/0000-0002-6821-9063>); Jothi Kesavan (<https://orcid.org/0000-0002-3266-9652>)

1. INTRODUCTION

Hastelloy C-2000 is widely used in the chemical industries, aeronautical, oil refining, industrial food sectors and anti-pollution systems. Alloy C-2000 outperforms common alloys like C-276 and can be used in place of alloy C-276 in many applications. It contains 1.6% copper, which is not present in alloy C-276 (Vara Prasad *et al.*, 2018). Hastelloy C-2000 has stronger mechanical and corrosion-resistant qualities, which allow it to be used for more applications (Hao *et al.*, 2021). Nickel, chromium, molybdenum, and a trace of copper compose the majority of the elemental composition of alloy C-2000 (Arulmurugan *et al.*, 2021a). The C-2000 alloy's outstanding corrosion resistance was due to its high Mo concentration, which can hinder corrosion growth and spread (Zhang *et al.*, 2013). Previous study indicated that the evaporation rate of Mo oxides is extremely fast over 725 °C, resulting in Mo element consumption in the composite (Birks *et al.*, 2006). Due to its remarkable performance in highly corrosive environments, the Hastelloy C-2000 alloy is a particularly interesting candidate material for high-temperature flue gas filters (Mcdaniel *et al.*, 2011; Li *et al.*, 2013). A vessel constructed of the alloy C-2000 may carry both oxidizing and reducing elements at the same time. It resists cracking, pitting, and stress corrosion cracking well (Pathak *et al.*, 2020). Alloy C-2000 may be welded using standard welding techniques. When traditional arc welding procedures such as TIG and MIG welding are performed, an excessive amount of heat is provided, greatly increasing the area of the heat-affected zone. More heat input results in a lesser depth of penetration (Prajapthi *et al.*, 2018). The mechanical qualities of a weldment are impacted not only by the composition of the parent metal but also by the weld bead geometry (Ma *et al.*, 2011). The bead on plate weld is a crucial feature of weld geometry, influencing chemical composition and the flux consumption rate of the weld zone and then determining the different mechanical properties of the weldment (Naffakh *et al.*, 2009).

The width of the weld bead is well recognised as a critical element influencing the geometrical characteristics of the weldment. The quality of the weldment is determined by satisfying requirements such as the geometry of the weld bead, which is impacted by various welding process parameters (Qiu *et al.*, 2020). It is probable that, for the examined set of input parameters, as current depths of penetration and reinforcement height grow, the weld bead width will increase to compensate for the increasing volume (Choudhary *et al.*, 2011). The intermetallics topologically close pack (TCP) phases, also known as Frank-Kasper (FK), promote hot cracking and early failure in weldments. The observed TCP phases are predominantly caused by the segregation of the alloying elements Mo and Cr (Manikandan *et al.*, 2014). From the observed research, the alloy C-2000 has good weld mechanical characteristics and microstructure, utilising autogenous and Mo-rich filler (ERNiCrMo-4) (Liu *et al.*, 2022). In both cases, the Cr-rich secondary TCP phases were found near the interdendritic area of the weld joints. As a result, mechanical characteristics deteriorated (Singh *et al.*, 2023). The production of secondary, brittle, and TCP phases during solidification is the main disadvantage of combining Ni-Cr-Mo alloys. During a eutectic reaction, most pure alloying elements surpass their solubility limits, causing the interdendritic area to separate (Arulmurugan *et al.*, 2021b). Improving the welding speed minimises the decomposition of the filler metal and the heat input per unit length of the weldment, resulting in smaller weld bead widths and weld reinforcement (Khanna and Maheshwari, 2016). Because of the heat energy transmitted to the base metal from the arc, weld bead width shrinks as welding speed increases (Mistry, 2016). Hastelloy C-2000 has superior properties and has undergone a variety of welding procedures. Gas tungsten arc welding (TIG) is an arc-based joining technology that creates an arc between a workpiece and a non-consumable tungsten electrode (Arulmurugan and Manikandan, 2018; Han *et al.*, 2020). Spin arc welding is used to increase the

productivity and quality of welding methods; it is also known as rotational arc welding. It is a welding technique that employs a one-of-a-kind welding gun and control system (Pathak *et al.*, 2020). The welding procedure is mostly carried out using gas metal arc welding (GMAW) with solid wires. In the industrial aspects of Hastelloy C-276, welding techniques such as gas metal arc welding (GMAW), gas tungsten arc welding (GTAW) and activated flux-TIG (A-TIG) welding are widely utilised (Yuquan *et al.*, 2014; Singh *et al.*, 2013). To enhance the microstructure of the welding zone, the process parameters are modified. To improve the quality of weldments with no secondary phases visible in the welding zone microstructure, electron beam welding and pulsed laser welding are used (Ahmad *et al.*, 2005). The spin arc welding technology intend to increase productivity by reducing the process duration and energy consumption in a corrosive environment (Câmpurean *et al.*, 2023).

To eliminate hot cracking, many methods such as pulsed current GTA, laser beam welding, and electron beam welding are utilised. Nonetheless, Spin Arc welding is a promising method in terms including both cost and effectiveness. The spin arc welding with bead on weld of Hastelloy C-2000 in-depth experiments were executed at minimal level to the researchers' knowledge. This research looks at the macro and microstructures of the weld interface, heat-affected zone (HAZ), and base metal. Several testing methods have been used to determine mechanical qualities such as hardness, tensile strength, and impact. The grain distribution in the weld zone and HAZ was analysed using FESEM. Also, the weld samples high intensity peak was determined using X-ray diffraction (XRD) analysis. The operations were performed with the following distinct parameter variations: speed, current, and spin diameter. Tensile strength, hardness, and impact strength were evaluated, and metallurgical characteristics were examined using an optical microscope and a FESEM.

Investigating the potential efficacy of the spin arc welding process on Hastelloy C-2000 was the main objective of this study.

2. MATERIALS AND METHODS

The Spin Arc welding was used for welding a Hastelloy C-2000 hot-rolled plate at a thickness of 2 mm. And the dimensions of the plate are 130×55×2 mm³ by using the filler ERNiCrMo-04 with a diameter of 1.2 mm. Table 1 show the welding parameters used during the procedure. Throughout the weld shown in Table 1, a constant travel speed of 300 mm·min⁻¹ was maintained. The Argon gas was delivered at a flow rate of 15 litres per minute for shielding and the back purging procedure. On each pass, a metal wire brush was utilized to remove the

contaminated oxide layer on the welding zone. Figure 2 in the ASTM standard for mechanical and metallurgical characterization depicts similar workpieces cut in the EDM process.

TABLE 1. Parameters of welding

Exp. No	Current (Amps)	Speed (r.p.m)	Spin dia (mm)	Travel speed (mm·min ⁻¹)
1.	120	1200	1	300
2.	120	1200	2	300
3.	120	1200	3	300
4.	120	1800	1	300
5.	120	1800	2	300
6.	120	1800	3	300
7.	120	2400	1	300
8.	120	2400	2	300
9.	120	2400	3	300
10.	140	1200	1	300
11.	140	1200	2	300
12.	140	1200	3	300
13.	140	1800	1	300
14.	140	1800	2	300
15.	140	1800	3	300
16.	140	2400	1	300
17.	140	2400	2	300
18.	140	2400	3	300
19.	160	1200	1	300
20.	160	1200	2	300
21.	160	1200	3	300
22.	160	1800	1	300
23.	160	1800	2	300
24.	160	1800	3	300
25.	160	2400	1	300
26.	160	2400	2	300
27.	160	2400	3	300

2.1. Metallurgy and Microstructure

The weld dimension of 10x10x2 mm was metallographically characterised, along with the normal direction of the weld joint. The polishing was carried out through three stages, with the first stage including the use of an emery sheet with grades ranging from 220 to 2000 grid. The second stage was completed using a disc polishing machine with water and alumina powder. The final stage of polishing used electrolytic cleaning with an oxalic acid solution.

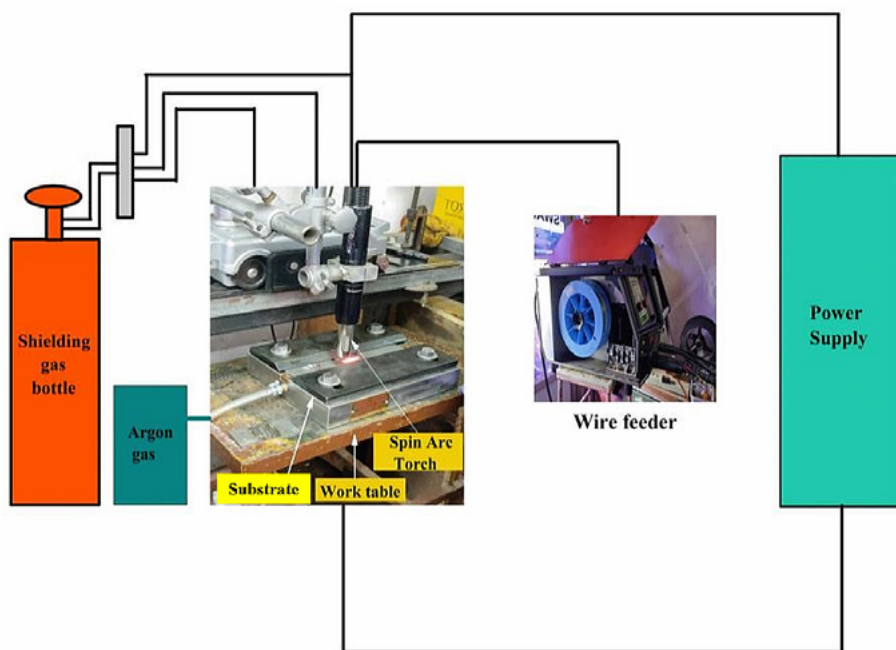


Figure 1 Experimental set-up of Spin Arc Welding.

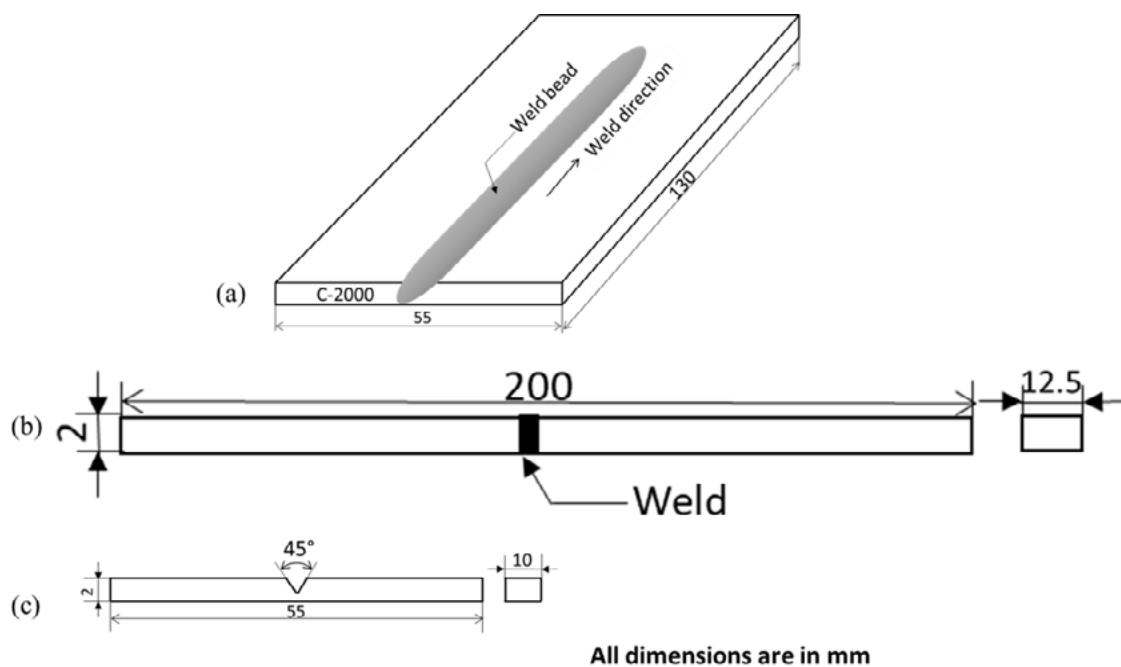


FIGURE 2. Schematic diagram of C-2000 (a) bead on plate weld; (b) tensile test specimen; (c) Impact test specimen.

The Optical Microscope (OM) and FESEM (Carl Zeiss Eigma TM equipment with 5kV and 10X - 1,000,000X magnification) were used to evaluate the microstructure of beads on welds. The X-Ray Diffraction test was used to identify crystal structural refinement and second phase and in the normal area of the fusion zone. Figure 1 depicts the entire experimental setup, which includes a wire feeder, shielding gas feeder, spin arc torch, and current supply.

2.2. Mechanical properties

The Vickers hardness test, the ultimate tensile strength test, and the Charpy impact test were used to determine mechanical strengths such as hardness, tensile strength, and toughness. Together with the weld bead, the testing coupons were moving in the cross-sectional direction. The tensile strength was determined using the Universal testing machine (UTM) and an extensometer. Table 2 shows the mechanical characteristics of the base metal.

The hardness of the weldment zone was measured using the Wolpert Wilson Vickers 452-SVD machine. The indenter was constructed of a diamond in the shape of a square pyramid. A conventional load of 500 g of force was given to a square pyramidal diamond indenter over the course of 20 seconds, at regular intervals of 2 mm. The experiment was repeated for each of the 27 samples. Figure 3 (a-b) also depicts the bead on plate weld joint workpiece that was utilised in this study. The Charpy V-notch test was employed to determine the overall energy absorbed in a weldment bead during the breakage. The V-notch was designed with a 45° angle to carry the impact weight. The

arm length in this test was 825 mm, the pendulum weight was 20.932 kg, and the pendulum release angle was maintained at 140°. In the merely supported state, the specimen's notch was positioned opposite the striking edge. To confirm the outcome and compute the average data, the measurements were tested several times.

3. RESULTS AND DISCUSSION

3.1. Macrostructural examination

The macro structural evaluation gave the penetration depth, width, height, and excess penetration, which are displayed in Fig. 4 (a-d) and Table 3. The grain size measurement and macrostructural analysis of comparable joints showed that all of the joints were effectively welded. Various welding parameters were employed to generate a similar weld, and the results were compared to another sample. Out of 27 samples, the Sample 5, and sample 15 had better penetration depth 2.493 and 2.450 mm, bead width 6.943 and 7.959 mm, bead height 4.687 and 4.887 mm and excess penetration 0.399 mm and 0.367mm with a current 120 and 140 I, speed 1800 r.p.m and spin diameter of 2 and 3 mm at constant travel speed of 300 mm·min⁻¹. There are no defects or cracks in the fusion zone or heat-affected zone of the weldments, and there is minimal excess penetration. The image and Table 3 shows the macrostructure and macrostructure interpretation of comparable weldments. A Dyni-lite digital microscope was used to capture macrostructure features of weldments. Additionally, the filler rod indicated that we employed the ERNiCrMo-04 filler material to accomplish

TABLE 2. Mechanical properties of Base metals

Base metal	Mechanical Properties			
	Hardness (HV)	Tensile strength (MPa)	Impact strength (J)	Percentage elongation
C-2000	185	753	462	61%

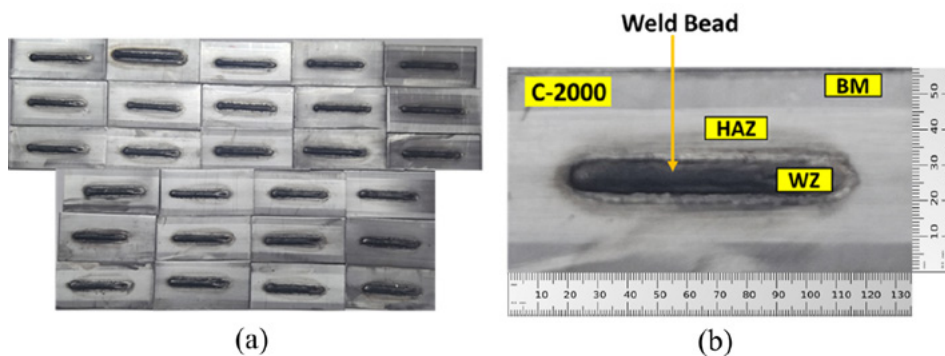


FIGURE 3. (a) C-2000 Bead on plate weld joints; (b) Different zones in C-2000 Bead on plate weld joint.

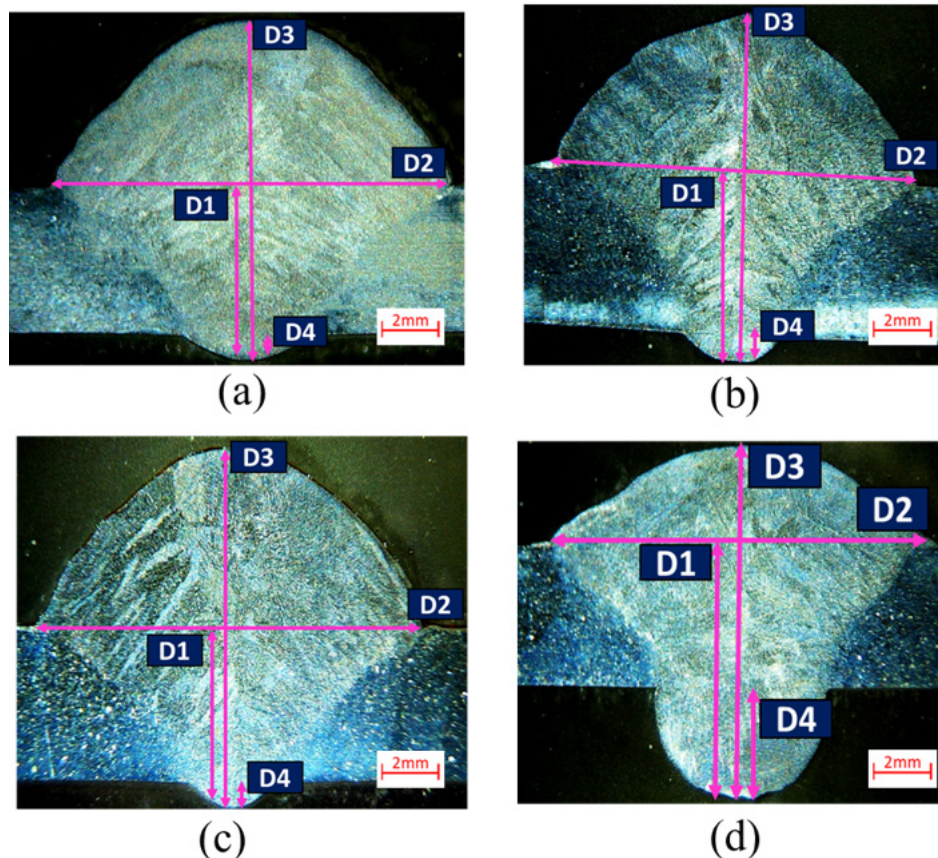


FIGURE 4. C-2000 Macrostructural examination of (a) sample 3; (b) sample 5; (c) sample 15 and (d) sample 22.

improved fusion and full penetration, resulting in a good base metal. The microstructure displayed the weldment's breadth and depth based on the various factors. A microscope was used to capture the macrostructural features of the weldments.

3.2. Optimal microstructure examination

The image depicts the optical microstructure analysis of Hastelloy C-2000 similar bead on plate welded joints. The weld zone microstructure is made up of equivalent dendrites, cellular grains, columnar dendrites, and columnar grains. The weld zone microstructure has fine equiaxed dendrites. The grain rough located adjacent to the heat-affected zone will be seen in the microstructure of alloy C-2000. Figure 5(a-m) depicts four distinct zones: base metals, heat-affected zones (HAZ), weld interfaces, and weld zones. The different tested sample microstructures are depicted in Fig. 5, with details exhibited at 100X magnification. The tiny grain size and dentition will be plainly seen under the microscope. The bead on plate welding will be performed using various parameters such as current, spinning speed, spinning diameter, and travel speed. In comparison to the other examples,

samples 5 and 15 were picked as the best since they were devoid of faults and cracks. The macrostructure examination (refer to Fig. 4) and macrostructure interpretation (refer to Table 2) were similar to the optical microstructure (OM) images. Additionally, it is consistent with improved grain size and dispersion being seen up to samples 5 and 15. Beyond samples 5 and 15, there are columnar dendrites and uneven grain development. As a result, it largely decreases the mechanical strength of joints.

3.3. Hardness test

The fusion zone has a somewhat greater average hardness rating than the basic metals. The enhancement is due to the presence of finer equiaxed grains in the weld zone. This is due to the fact that filler wire contains additional alloy elements that drive the solution-strengthening impact. The mean hardness values of the alloy C-2000 were determined and compared to the welded samples' least and highest values. Samples 5 and 15 have a higher hardness value because of their finer equiaxed grains. Also, it has higher tensile and impact strength compared to the remaining samples. Similarly, sample 22 hardness rating was deter-

TABLE 3. Interpretation of Macro Examination

Samples	Penetration Depth (D1) (mm)	Width (D2) (mm)	Height (D3) (mm)	Excess Penetration (D4) (mm)
1	1.972	6.759	5.348	1.132
2	3.458	7.068	5.865	1.375
3	2.451	6.631	4.877	0.399
4	1.949	4.687	3.879	0.392
5	2.493	6.943	4.687	0.399
6	1.330	7.841	3.675	---
7	3.773	9.192	6.414	1.705
8	2.377	7.006	4.789	0.335
9	0.760	7.559	3.086	---
10	2.603	8.210	4.619	0.555
11	4.706	8.595	5.941	1.523
12	2.035	6.710	4.650	0.158
13	3.397	6.722	5.558	0.876
14	2.710	8.083	4.876	1.353
15	2.450	7.959	4.887	0.367
16	3.308	7.653	5.008	1.248
17	2.427	7.014	4.363	0.586
18	2.265	7.845	4.137	0.390
19	2.325	7.267	4.610	0.570
20	2.911	7.580	5.320	0.861
21	3.160	7.959	5.188	1.295
22	3.702	7.671	5.264	0.865
23	2.217	8.758	4.719	1.651
24	2.145	6.679	4.563	0.264
25	2.709	8.296	4.808	0.646
26	2.504	7.497	4.645	0.658
27	2.636	9.826	4.976	0.651

mined to be an intermediate value, with fine equiaxed grains. Table 4 shows that sample 3 has a lower hardness value due to its inadequate equiaxed grain size. These changes in hardness value are generated by varying welding parameters (shown in Table 1). The hardness of the weld bead is steadily increases in the HAZ, reaching its maximum value at the weld FZ. The hardness value is measured at a certain distance (2 mm) from the left, right, and FZ (fusion zone) of bead on plate weldments.

3.4. Tensile test

In this research, the tensile test results of weldments were achieved in this study by employing universal testing equipment under certain loading condi-

tions. By establishing a weld microstructure with an equiaxed grain pattern, the mechanical properties of various coordinate axes of X, Y, and Z will be similar in all three directions. It also maintains isotropic characteristics. Because of the existence of a high quantity of fine equiaxed grains size in the FZ of bead on weld, the tensile strength has been improved. Similarly, the spacing between dendrite arms is maintained equally in all directions. Fine equiaxed grains are more ductile than columnar grains. As a result, fine equiaxed grains can deform rapidly while resisting contraction stresses. As a result, equiaxed grains prevent FZ failure and can sustain tensile loads well. In this study, of the 27 samples, sample 5 and sample 15 had the highest UTS (refer Fig. 6). Because of the higher hardness values of the samples the ultimate

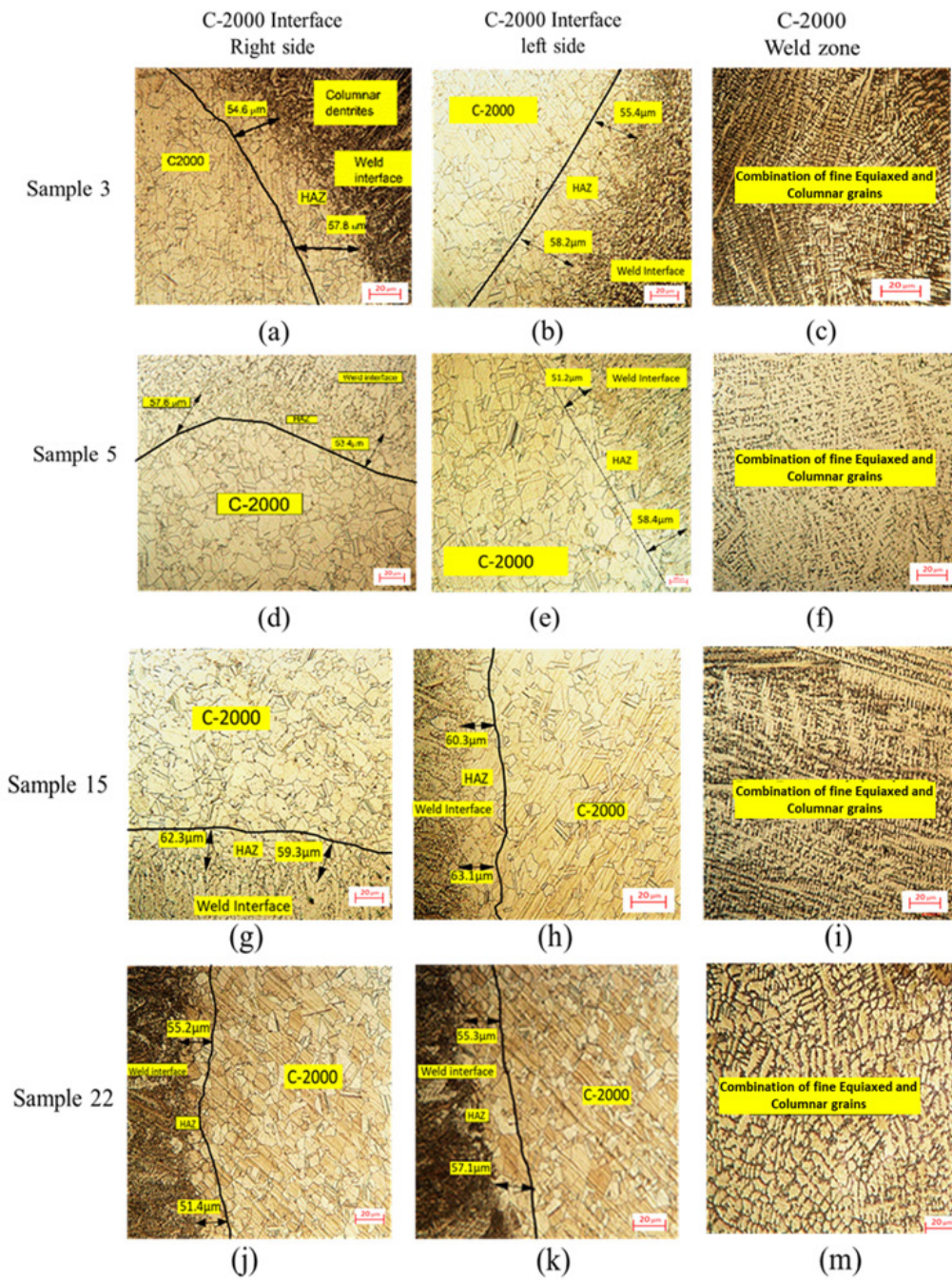


FIGURE 5. C-2000 Microstructural Examination in interface of right side, left side and weld zone in the sample 3 (a, b, c); sample 5 (d, e, f); sample 15 (g, h, i) and sample 22 (j, k, m).

TABLE 4. Comparison of Hardness Values

Sample	Current (I)	Spinning Speed (rpm)	Travel speed mm·min ⁻¹	Spin diameter (mm)	Hardness value (HV)	Hardness value range
5	120	1800	300	2	272	Higher
15	140	1800	300	3	272	Higher
22	160	1800	300	1	252	Intermediate
3	120	1200	300	3	238	Lower

tensile strength will be enhanced upto 7.9% compared to MPCGTAW-ERNiCrMo-17 weldment. The fusion zone tensile properties will be improved by the reduced heat input, increased cooling rate, and the absence of microsegregation, resulting in a finer microstructure. The development of Mo-rich secondary phases in the interdendritic zones indicates a reduction in the strength and flexibility of the weld joints during spin arc welding FESEM fractography has revealed the ductility of the tensile fractures by exhibiting a significant number of micro-voids with ductile tearing ridges that should have failed due to crystallisation mechanism failure. Moreover, the development of more micro-voids with long dimples and lower cleavage facets indicates a ductile mode of failure. The dimension of the ductile dimple varies in each sample used for fractography.

3.5. Impact test

The Charpy V-notch test was used to determine the impact toughness of the weldments. These ex-

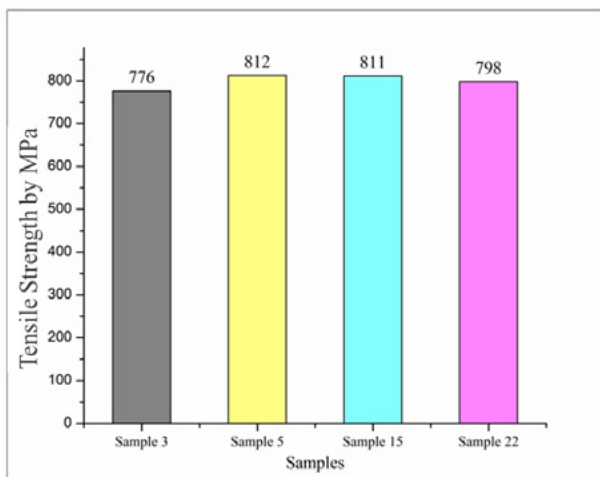


FIGURE 6. Tensile strength in MPa.

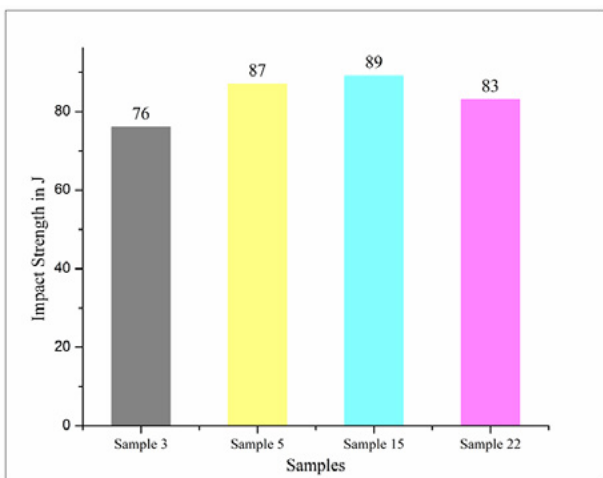


FIGURE 7. Impact Strength in J.

periments were carried out to determine the impact values for a bead on plate weld of alloy C-2000. The impact values in Joules (J) were acquired from the test. Moreover, this test was carried out at ambient temperature. Of the 27 samples, samples 5 and 15 are the best; as compared to alloy C-2000, the toughness of welded FZ is 23.68% lower. This is because to a lack of alloying element microsegregation at both bead weld interfaces and FZ. It also withstands impact loads well because to the existence of equiaxed grains with fine microstructures. As compared to the MPCGTAW-ERNiCrMo-17 approach, the toughness of samples 5 and sample 15 is 5.9% higher. It has high impact strength, as demonstrated in Fig. 7, and performs better in all other strength tests, including the tensile strength test and the hardness test (see Fig. 6 and Table 3). It also contains fine equiaxed grains. The observed tensile and impact strength data have been compared to earlier studies, as shown in Table 5.

3.6. XRD analysis

Figure 8 depicts the use of X-ray diffraction (XRD) to assess the phase study composition and the aver-

TABLE 5. Comparative analysis of Tensile and impact strength

Welding method	Ultimate tensile strength (UTS) (MPa)	Toughness (Impact test) in J	Reference
Alloy C-2000	1046	114	(Arulmurugan <i>et al.</i> , 2021a)
MPCGTAW-ERNiCrMo-17	783	84	
Spin arc welding ERNiCrMo-4	815	89	-

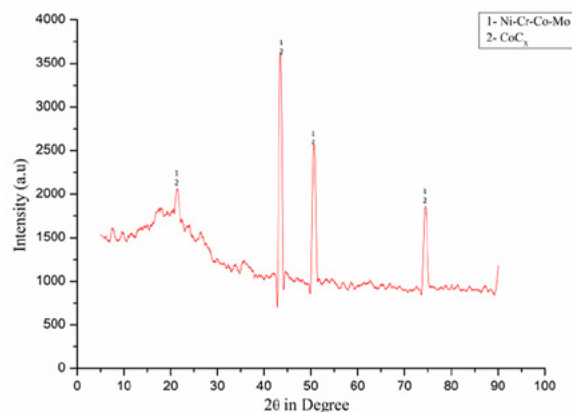


FIGURE 8. The XRD analysis of the sample 5

age grain size of the bead on weld of sample 5. The XRD analysis will reveal the high-intensity peaks (Ni-Cr-Co-Mo) and (CoCx) of the welded zone. The elemental development and precipitates (Ni, Cr, Co, and Mo) will increase the performance of the bead on the weld and prevent cracks from forming in the fusion zone. These precipitates keep them from expanding and shattering. The segregation of molybdenum and chromium-rich precipitates is not apparent in XRD results. The XRD investigations are repeated for the twenty-seven samples and compared to one another in order to choose more effective work settings. In comparison to the other twenty-seven samples, samples 5 had average grain size and phase composition values. The results reveal that a crack-free weld increases the strength of the samples. It is believed that the Spin Arc Welding parameter does not allow for the segregation of molybdenum and chromium-rich components in interdendritic areas. This is due in part to the Spin Arc Welding minimal heat input, rapid cooling rate, and considerable thermal gradient.

3.7. FESEM analysis

The FESEM analysis is carried out at the best magnification ratio possible, and a grid matrix is started to obtain current FESEM pictures in various areas. The Fig. 9(a-h) shows a higher magnification FESEM micrograph of the bead weld fusion zone used in the investigation. Figure is shown bead weld FZ with exquisite equiaxed dendritic structure. The necessary elemental values (Ni, Cr, Co, Mo, and CoCX) are found at the bead on weld unique zone, and the welding zone has a fine columnar and equiaxed dendritic structure. FESEM was used to examine the lack of a secondary topologically closed packed (TCP) phase at the weld centre. There is no evidence of a significant secondary TCP phase in the interface region between the similar alloy C-2000 and the bead on the weld. This indicates that there is no hot cracking and no defects are present in the bead on plate welds. Samples 5 and 15 are chosen as the best in Spin Arc Welding because of their low level currents (120 I and 140 I), medium spinning speed (1400 rpm), and small spin diameters (2 and 3 mm), which have greater mechanical qualities and more evenly distributed grains than the other welding parameters. The spin arc energy may be successfully exploited to join the targeted region in a short period by conductivity into the base metal. Due of the decreased rapid cooling rate and heat input, the weld interface and fusion zone do not have enough time to separate the alloying components.

4. CONCLUSION

Selective parameters including current, spinning speed, and spin diameter were used to create a defect-free weld on a Hastelloy C-2000 bead using spin

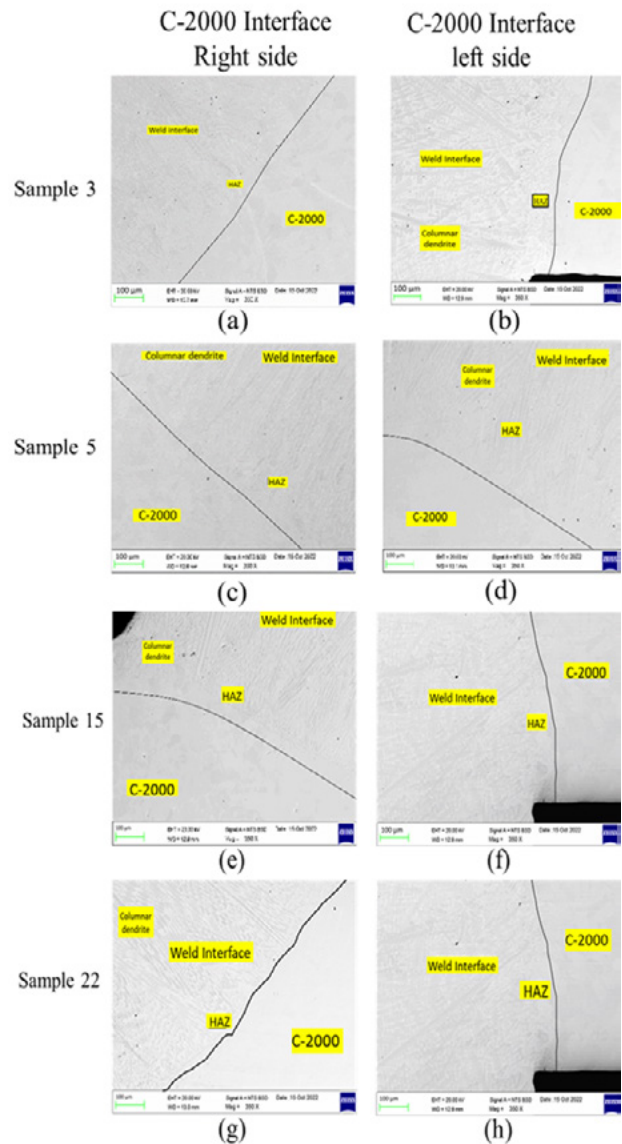


FIGURE 9. C-2000 FESEM analyses in interface of right side and left side of the sample 3 (a, b); sample 5 (c, d); sample 15 (e, f); sample 22 (g, h).

arc welding and filler wire constructed of ERNiCrMo-4.

- As compared to the weld zone, the base metals C-2000 was noted to have higher hardness values. Samples 5 and 15 yielded the higher hardness values of 272 HV and 272 HV, respectively, while sample 3 yielded the lower hardness value of 238 HV.
- Compared to MPCGTAW-ERNiCrMo-17, the spin arc welding samples' ultimate tensile strength have been noted to be increased by 7.9% in bead on weld of Hastelloy C-2000. This is because the samples had a higher surface hardness levels.

- The Charpy test was conducted after the impact test at room temperature. The impact values determined from the test were 89 J and 88 J for sample 5 and 15, respectively. Samples 5 and 15 exhibited the best toughness values, and it was 5.7% greater in spin arc welding compared to the MPCGTAW-ERNiCrMo-17 technique.
- FESEM investigation revealed that there was no secondary TCP at the weld centre, confirming that there was no hot cracking in the weldments. Because of the decreased heat input and rapid cooling rate, the weld interface and fusion zone did not have enough time to separate the alloying components.

Nomenclature

1. EDS – Energy Dispersive x-ray Spectrograph
2. XRD – X – Ray Diffraction
3. UTS – Ultimate Tensile Strength
4. MPCGTAW – Multi-pass Pulsed Current Gas Tungsten Arc Welding
5. GTAW – Gas Tungsten Arc Welding
6. GMAW – Gas Metal Arc Welding
7. SMAW – Shielded Metal Arc Welding
8. PAW – Plasma Arc Welding
9. EBW – Electron Beam Welding
10. LBW – Laser Beam Welding
11. FGD – Flue Gas Desulphurization
12. FZ – Fusion Zone
13. HAZ – Heat Affected Zone
14. ASTM – American Society for Testing and Material
15. FESEM – Field Emission Scanning Electron Microscope

Disclosure of potential conflicts of interest

The authors declare that they have no conflict of interest.

ACKNOWLEDGMENTS

The authors convey their sincere gratitude to Prof. Balakumar Pitchai, Director of ‘Centre for Scholarly Scientific Training and Publishing’, and Prof. Kumaran Shanmugam, Dean Research, Periyar Maniammai Institute of Science & Technology (Deemed-to-be university), Vallam, Tanjavur, Tamil Nadu, India, for their timely help in language editing and critical reading of the manuscript.

REFERENCES

Ahmad, M., Akhter, J.I., Akhtar, M., Iqbal, M., Ahmed, E., Choudhry, M. (2005). Microstructure and hardness studies of the electron beam welded zone of Hastelloy C-276. *J. Alloys Compd.* 390 (1-2), 88–93. <https://doi.org/10.1016/j.jallcom.2004.08.031>.

Arulmurugan, B., Manikandan, M. (2018). Improvement of metal-lurgical and mechanical properties of gas tungsten arc weldments of Alloy 686 by current pulsing. *Trans. Indian Inst. Met.* 71, 2953–2970. <https://doi.org/10.1007/s12666-018-1395-8>.

Arulmurugan, B., Sathish Kumar, M., Balaji, D., Muralikrishnan, K., Pranesh, S., Praveen, V., Praveen Kumar, K., Arivazhagan, N., Manikandan, M. (2021a). Development to arc welding technique to preclude microsegregation in the dissimilar joint of Alloy C-2000 and C-276. *P. I. Mech. Eng. Part E: J. Process Mech. Eng.* 235 (5), 1408–1419. <https://doi.org/10.1177/09544089211000011>.

Arulmurugan, B., Sathish Kumar, M., Kannan, T., Karupiah, S., Kumaraguru, N., Ponsundar, E., Raghu, G., Manikandan, M. (2021b). Investigation on mechanical and microstructure characteristics of nickel based C-2000 super alloy using laser beam welding. *Mater. Today Proc.* 43 (5), 3044–3049. <https://doi.org/10.1016/j.matpr.2021.01.393>.

Birks, N., Meier, G.H., Pettit, F.S. (2006). *Introduction to the high-temperature oxidation of metals*. 2nd edición, Cambridge University Press. <https://doi.org/10.1017/CBO9781139163903>.

Câmpurean, A.M., Sirbu, N.A., Verbiţchi, V., Duma, J., Popescu, R.N. (2023). Development of a Gas-Metal-Arc Welding Technology with Combined Spin-Arc and Weaving Facilities for Ship Building. *Mater. Sci. Forum* 1095, 59–68. <https://doi.org/10.4028/p-we4fLO>.

Choudhary, D., Jindal, S., Mehta, N.P. (2011). To study the effect of welding parameters on weld bead geometry in SAW welding process. *Elixir Mech. Engg.* 5519–5524. <https://www.researchgate.net/publication/272510315>.

Han, D., Wei, J., Wang, S., Pan, Y., Xue, J., Wei, Y. (2020). Feather-like NiCo₂O₄ self-assemble from porous nanowires as binder-free electrodes for low charge transfer resistance. *Front. Mater. Sci.* 14, 450–458. <https://doi.org/10.1007/s11706-020-0528-2>.

Hao, C., Li, K., Jincheng, P., Boce, X., Dong, D., Baohua, C. (2021). Effect of the welding position on weld quality when laser welding Inconel 617 Ni-based super alloy. *Opt. Laser Technol.* 139, 106962. <https://doi.org/10.1016/j.optlastec.2021.106962>.

Khanna, P., Maheshwari, S. (2016). Effect of Welding Parameters on Weld Bead Characteristics during MIG Welding of Stainless Steel 409M. *J. Prod. Eng.* 19 (2), 43–48.

Li, X.M., Bai, J.W., Liu, P.P., Zhu, Y.M., Xie, X.S., Zhan, Q. (2013). Coherent Ni, (Cr, Mo) precipitates in Ni–21Cr–17Mo superalloy. *J. Alloys Compd.* 559, 81–86. <https://doi.org/10.1016/j.jallcom.2013.01.098>.

Liu, X., Guo, Y., Zhang, W., Wu, D., Huang, R., Yang, M., Lu, B. (2022). Dynamic formation characteristics and mechanism of hybrid laser arc welding surface layer by Ni-based filler metal based on rotating laser induction. *J. Mater. Res. Technol.* 20, 3600–3615. <https://doi.org/10.1016/j.jmrt.2022.08.121>.

Ma, G., Wu, D., Guo, D. (2011). Segregation characteristics of pulsed laser butt welding of Hastelloy C-276. *Metall. Mater. Trans. A* 42 (13), 3853–3857. <https://doi.org/10.1007/s11661-011-0978-3>.

Manikandan, M., Arivazhagan, N., Rao, M.N., Madhusudhan Reddy, G. (2014). Microstructure and mechanical properties of alloy C-276 weldments fabricated by continuous and pulsed current gas tungsten arc welding techniques. *J. Manuf. Processes* 16 (4), 653–572. <https://doi.org/10.1016/j.jmapro.2014.08.002>.

Mcdaniels, R.L., Chen, L., Steward, R., Liaw, P.W., Buchanan, R.A., Steve, W., Kelvin, L., Klarstrom, D.L. (2011). The strain-controlled fatigue behavior and modeling of Hastelloy C®-2000® superalloy. *Mater. Sci. Eng. A* 528 (12), 3952–3960. <https://doi.org/10.1016/j.msea.2010.10.024>.

Mistry, P.J. (2016). Effect of Process Parameters on Bead Geometry and Shape Relationship of Gas Metal Arc Weldments. *Int. J. Adv. Res. Mech. Eng. Technol.* 2, 24–27.

Naffakh, H., Shamanian, M., Ashrafzadeh, F. (2009). Dissimilar welding of AISI 310 austenitic stainless to nickel based alloy Inconel 657. *J. Mater. Process. Technol.* 209 (7), 3628–3639. <https://doi.org/10.1016/j.jmatprotec.2008.08.019>.

Pathak, U., Taiwade, R.V., Balbande, S. (2020). Weldability of bi-metallic butt joint between hastelloy C-276 and advance austenitic stainless steel. *Mater. Today: Proc.* 28 (4), 2547–2550. <https://doi.org/10.1016/j.matpr.2020.05.114>.

- Prajapati, P., Badheka, V.J., Mehta, K. (2018). An outlook on comparison of hybrid welds of different root pass and filler pass of FCAW and GMAW with classical welds of similar root pass and filler pass. *Sadhana* 43 (75), 1-10. <https://doi.org/10.1007/s12046-018-0869-z>.
- Qiu, Z., Wu, B., Zu, H., Wang, Z., Hellier, A., Ma, Y., Li, H., Muransky, O., Wexler, D. (2020). Microstructure and mechanical properties of wire arc additively manufactured Hastelloy C276 alloy. *Mater. Des.* 195, 109007. <https://doi.org/10.1016/j.matdes.2020.109007>.
- Singh, R.P., Gupta, R.C., Sarkar, S.C. (2013). Prediction of Weld Width of Shielded Metal Arc Weld under Magnetic Field using Artificial Neural Networks. *Int. J. Comput. Eng. Res.* 3 (1), 58–64. <https://doi.org/10.13140/RG.2.2.15848.67845>.
- Singh, A., Singh, V., Singh, A.P., Patel, D., Gupta, S.K. (2023). Experiment analysis of A-TIG welding and comparison between TIG, Double-TIG, and A-TIG of Hastelloy C-276. *Mater. Today: Proc.* (In Press). <https://doi.org/10.1016/j.matpr.2023.05.199>.
- Vara Prasad, V., Madhu Babu, C., Ajay, P. (2018). A Review on Rotating Arc Welding Process. *Mater. Today: Proc.* 5 (2), 3551–3555. <https://doi.org/10.1016/j.matpr.2017.11.603>.
- Yuquan, G., DongJiang, W., Guangyi, M., Dongming, G. (2014). Numerical simulation and experimental investigation of residual stresses and distortions in pulsed laser welding of Hastelloy C-276 thin sheets. *Rare Metal Mater. Eng.* 43 (11), 2633-2668. [https://doi.org/10.1016/S1875-5372\(15\)60022-4](https://doi.org/10.1016/S1875-5372(15)60022-4).
- Zhang, X., Zagidulin, D., Shoesmith, D.W. (2013). Characterization of film properties on the Ni–Cr–Mo alloy C-2000. *Electrochim. Acta* 89, 814–822. <https://doi.org/10.1016/j.electacta.2012.11.029>.